Preprints.org

Article

Not peer-reviewed version

Glass Microfluidic Bioelectrochemical Cell Platform for the Study of Extracellular Electron Uptake in Microbes

Andreea Stoica , Karthikeyan Rengasamy , Tahina O. Ranaivoarisoa , Joshua A. Van Dyke-Blodgett , Arpita Bose * , J. Mark Meacham *

Posted Date: 13 April 2026

doi: 10.20944/preprints202505.1879.v2

Keywords: glass microfluidics; scalable microfluidics; microfluidic bioelectrochemical cell; extracellular electron uptake; *Rhodopseudomonas palustris* TIE-1

Preprints.org is a free multidisciplinary platform providing preprint service that is dedicated to making early versions of research outputs permanently available and citable. Preprints posted at Preprints.org appear in Web of Science, Crossref, Google Scholar, Scilit, Europe PMC.

Copyright: This open access article is published under a Creative Commons CC BY 4.0 license, which permit the free download, distribution, and reuse, provided that the author and preprint are cited in any reuse.

Preprints.org (www.preprints.org) | NOT PEER-REVIEWED | Posted: 13 April 2026 doi:10.20944/preprints202505.1879.v2

Disclaimer/Publisher's Note: The statements, opinions, and data contained in all publications are solely those of the individual author(s) and contributor(s) and not of MDPI and/or the editor(s). MDPI and/or the editor(s) disclaim responsibility for any injury to people or property resulting from any ideas, methods, instructions, or products referred to in the content.

Article

Glass Microfluidic Bioelectrochemical Cell Platform for the Study of Extracellular Electron Uptake in Microbes

Andreea Stoica [1], Karthikeyan Rengasamy [2], Tahina O. Ranaivoarisoa [2], Joshua A. Van Dyke-Blodgett [2], Arpita Bose [2,*] and J. Mark Meacham [1,*]

[1] Department of Mechanical Engineering and Materials Science, Washington University in St. Louis, Missouri, USA

[2] Department of Biology, Washington University in St. Louis, Missouri, USA

* Correspondence: abose@wustl.edu (A.B.); meachamjm@wustl.edu (J.M.M.); Tel.: +1-314-935-6236 (A.B.); +1-314-935-3821 (J.M.M.)

Abstract

Miniaturization of microfluidic measurement systems offers several advantages, including reduced sample and reagent volumes, improved control over experimental conditions, and the ability to multiplex complementary measurement modalities, to enable new experimental approaches in microbial electrochemistry. We present a scalable glass-based microfluidic bioelectrochemical cell (μ-BEC) platform for multiplexed investigations of microbial extracellular electron uptake (EEU). The platform integrates eight independently addressable three-electrode cells in a 2×4 array, with transparent indium tin oxide working electrodes that support simultaneous electrochemical analysis and optical imaging. Systematic electrochemical characterization using the ferri/ferrocyanide redox couple demonstrated diffusion-controlled behavior and stable reference electrode performance, with well-to-well coefficients of variation in peak potentials of 0.6–1.5% and 0.6–1.1% for anodic and cathodic processes and device-to-device coefficients of variation of approximately 1.8% and 1.6%, respectively. Differential pulse voltammetry measurements demonstrated concentration-dependent electrochemical sensing over a three-order-of-magnitude range from 1 μM to 1 mM ferri/ferrocyanide, with peak currents exhibiting linear dependence on concentration for both anodic and cathodic processes across all tested wells. Biological compatibility was validated using the phototrophic bacteria *Rhodopseudomonas palustris* TIE-1, where reproducible light-dependent EEU was observed following 96 hours of incubation, and a reduction in current response after microfluidic removal of planktonic cells confirmed the contribution of surface attached cells to EEU. Together, these results establish the μ-BEC as a robust and reproducible microfluidic electrochemical platform suitable for parallelized, multimodal studies of microbial and abiotic electrochemical processes.

Keywords: glass microfluidics; scalable microfluidics; microfluidic bioelectrochemical cell; extracellular electron uptake; *Rhodopseudomonas palustris* TIE-1

1. Introduction

Most life forms rely on oxidation-reduction reactions for energy generation, and such processes generally involve the transfer of electrons from donor to acceptor chemical species. Many familiar microbes utilize soluble electron donors or acceptors. However, in environments where these are limited, some microbes have evolved the ability to transfer electrons to or from external solids. Known as extracellular electron transfer (EET), this adaptation enables microbes to access critical energy resources in otherwise redox-limited environments in deep marine sediments, anoxic soils, and the mineral-rich subsurface (Lovley and Holmes 2022; Shi et al. 2016). EET is theoretically a bidirectional process, so specifying the direction of electron flow is essential for descriptive accuracy

© 2026 by the author(s). Distributed under a Creative Commons CC BY license.

Preprints.org (www.preprints.org) | NOT PEER-REVIEWED | Posted: 13 April 2026 doi:10.20944/preprints202505.1879.v2

(Conners et al. 2022). In reductive extracellular electron transfer (rEET), electrons are transported out of the cell to reduce external solid-phase electron acceptors, e.g., in *Geobacter sulfurreducens* (Lovley et al. 1987) reduction of Fe(III) oxides. Conversely, extracellular electron uptake (EEU) involves the flow of electrons into the cell from external solid-phase electron donors. Photoautotrophic bacteria, such as *Rhodopseudomonas palustris* (Guzman et al. 2019), can couple EEU with CO_2 fixation, to allow the synthesis of biomass from inorganic carbon.

EET has far-reaching significance in both ecological and biotechnological contexts. In natural systems, it plays a crucial role in microbial energy flow and biogeochemical cycling, particularly in anoxic and nutrient-limited environments (Lovley and Holmes 2022). Beyond its importance in nature, EET has substantial potential for applications in biotechnology and sustainable development. Microbes capable of EET are instrumental in bioremediation, where they facilitate the removal or immobilization of environmental pollutants. Examples include species such as *Geobacter* that reduce and immobilize toxic metals like uranium by transferring electrons to insoluble electron acceptors (Cologgi Dena et al. 2014; Lovley et al. 1991). Elsewhere, microbial fuel cells (MFCs) generate renewable electrical energy by harnessing rEET via the microbial oxidation of organic matter, where resultant electrons are transferred to an anode. (Franks and Nevin 2010; Lovley 2006). Microbial electrosynthesis (MES) represents another significant application of EET, specifically EEU. In MES systems, microbes accept electrons from a cathode to reduce carbon dioxide and divert this biomass into value-added bioproducts, including biofuels, bioplastics, and specialty chemicals (Karthikeyan et al. 2019; Lovley and Nevin 2013; Nevin Kelly et al. 2010). For example, by coupling EEU with light-driven carbon fixation, photoautotrophic microbes create carbon-neutral pathways to produce sustainable bioproducts (Ranaivoarisoa et al. 2019).

Conventional electrochemical systems used to study EET in the laboratory are limited in their adaptability to high-throughput and multiplexed experimentation. Their size and complexity preclude multiplexing possibilities, increase reagent consumption, and constrain the parallel electrochemical measurements needed to compare conditions or screen large bacterial libraries efficiently. The limitations of macroscale reactors for EET studies have driven a growing call for miniaturization, and a range of miniaturized electrochemical platforms have since been developed to address them (Parkhey and Sahu 2021; Pinck et al.; Yang et al. 2016). Miniaturized alternatives include paper-based microbial fuel cell arrays (Tahernia et al. 2020a; Tahernia et al. 2019, 2020b), flexible textile-based systems (Kim et al. 2024; Kwon et al. 2024; Park et al. 2023), and polydimethylsiloxane (PDMS)-based devices (Amirdehi et al. 2022; Gong et al. 2022; Khodaparastasgarabad et al. 2024; Zarabadi et al. 2017). Carbon nanotube (CNT)-modified electrodes have improved biofilm-electrode interactions in confined systems (Cho et al. 2022; Lee et al. 2023), while integrated LED-based circuits have simplified electrogenicity screening in resource-limited settings (Cho et al. 2022). Despite this progress, the fabrication of miniaturized bioelectrochemical reactors remains constrained by trade-offs between scalability, cost, and compatibility with imaging and other measurement workflows. Similar to other miniaturized microfluidic applications, realizing the full potential of these platforms will require fabrication strategies that are scalable, optically compatible, and lower the barrier to high-throughput widespread adoption(Battat et al. 2022; Sackmann et al. 2014).

Here, we introduce a scalable, glass-based microfluidic bioelectrochemical cell (μ-BEC) platform that enables reproducible, multiplexed, imaging-compatible electrochemical measurements at the microscale. The μ-BEC integrates eight three-electrode cells featuring transparent working electrodes in a 2 × 4 well layout combined with exquisite microfluidic control (Figure 1). Rigorous validation by a variety of methods (e.g., cyclic voltammetry and chronoamperometry), including the ferricyanide/ferrocyanide redox couple, demonstrated diffusion-controlled behavior, stable reference electrode performance, and reproducibility between wells and across individual devices. Differential pulse voltammetry measurements established the μ-BEC capacity to support concentration-dependent electrochemical sensing under abiotic conditions, and the biocompatibility of the platform

© 2026 by the author(s). Distributed under a Creative Commons CC BY license.

Preprints.org (www.preprints.org) | NOT PEER-REVIEWED | Posted: 13 April 2026 doi:10.20944/preprints202505.1879.v2

was demonstrated by observing *Rhodopseudomonas palustris* TIE-1 light-dependent extracellular electron uptake.

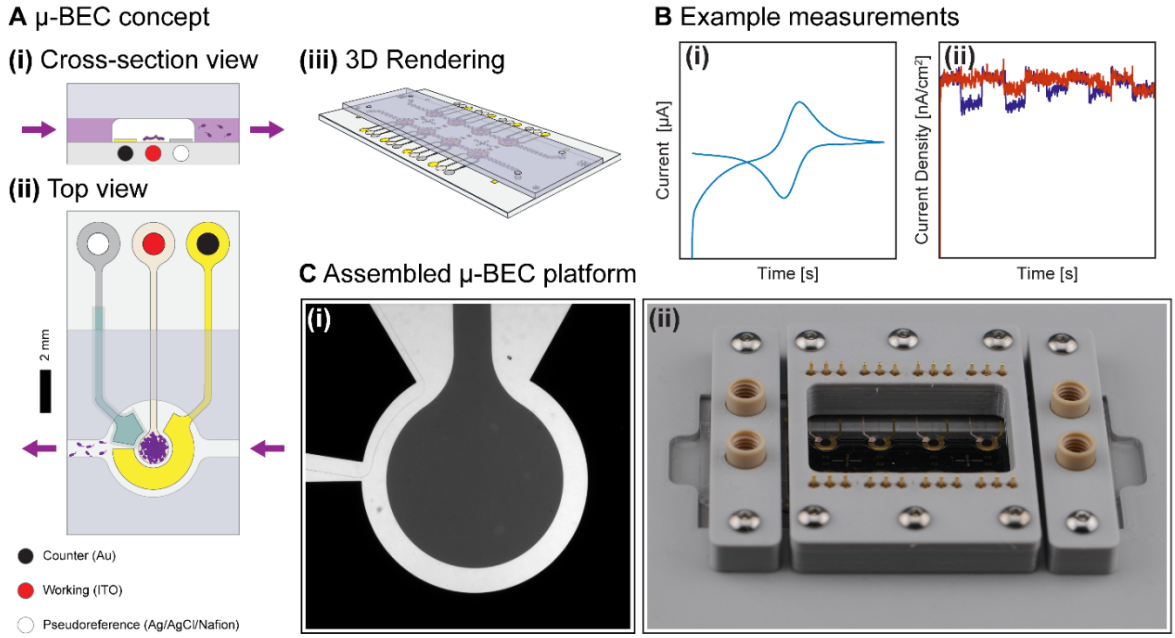

Figure 1. Microfluidic bio-electrochemical cell (μ-BEC) platform. (A) Motivation behind μ-BEC platform development (i) cross-section view, (ii) top view (iii) 3D rendering of μ-BEC platform; (B) Example (i) cyclic voltammetry and (ii) light on/off chronoamperometry measurements (C) Fabricated μ-BEC device (i) inset of fabricated unit cell and (ii) assembled platform inside the microscopy and electrochemical measurements compatible holder.

2. Materials and Methods

2.1. Design and Fabrication of the μ-BEC Devices

The μ-BEC fabrication steps are illustrated in Figure S1 and Figure S2. Process descriptions are summarized here. Aligned electrode layers were fabricated on clean 100-mm diameter, 500-μm thick borosilicate glass wafers (University Wafer, Boston, MA) using a series of lift-off processes (KL8020 HMDS primer, KemLab™, Livermore, CA; 1.5-μm thick LOR 10B lift-off resist and 0.6 μm Microposit™ S1805™, Kayaku Advanced Materials Inc., Westborough, MA). Electrode patterns were exposed by direct laser writing (DWL 66+, Heidelberg Instruments Mikrotechnik GmbH, Heidelberg, Germany) and developed using Microposit™ MFR-319 developer (Kayaku Advanced Materials Inc.) with residual photoresist removed by 10-s exposure to a 100-W ozone plasma (PE-50 Plasma Asher, Plasma Etch Inc., Carson City, NV).

Counter electrodes and alignment marks were deposited by thermal evaporation (20-nm thick Cr adhesion layer and 250-nm thick Au, AUTO 306 Vacuum Coater, Edwards Vacuum, West Sussex, UK). Working electrodes were deposited by magnetron sputtering (250-nm thick indium tin oxide (ITO), PVD 75, Kurt J. Lesker, Jefferson Hills, PA). Pseudoreference electrodes were deposited by sequential magnetron sputtering (30-nm thick Ti adhesion layer and 1000-nm thick Ag, PVD 75, Kurt J. Lesker). After each electrode deposition, lift-off was performed by immersion in a 65 °C Remover PG bath (Kayaku Advanced Materials Inc.) for 1 h, followed by transfer to a fresh room-temperature Remover PG bath for at least 12 h. Wafers were vacuum annealed at 320 °C and 1 × 10^{-6} Torr for 30 min, then cooled to room temperature under argon (20 mTorr, 220 sccm) to enhance electrode adhesion and reduce the working electrode sheet resistance.

The pseudoreference electrodes were further modified through a solution-based chlorination method to create a silver chloride (AgCl) layer. Working and counter electrodes were protected

© 2026 by the author(s). Distributed under a Creative Commons CC BY license.

Preprints.org (www.preprints.org) | NOT PEER-REVIEWED | Posted: 13 April 2026 doi:10.20944/preprints202505.1879.v2

during chlorination by a layer of AZ P4620 photoresist (MicroChemicals GmbH, Ulm, Germany). Exposed pseudoreference electrodes were cleaned in 10% hydrochloric acid (HCl), chlorinated in a 50 mM ferric chloride ($FeCl_3$) aqueous solution for 50 s, stabilized in a 3.5 M potassium chloride (KCl) aqueous solution for 5 s, and rinsed in deionized (DI) water. The protective AZ P4620 photoresist was subsequently removed by sequential washing in acetone, methanol, and isopropanol, before drying under nitrogen flow. Subsequently, the pseudoreference electrodes were coated with a protective Nafion™ layer using a sacrificial PDMS microfluidic channel designed to selectively expose only the pseudoreference electrode surface while shielding the working and counter electrodes. PDMS channels were fabricated by standard soft lithography using a 100-µm thick SU-8 2100 photoresist replica mold (Kayaku Advanced Materials Inc.). After punching 1-mm diameter inlet and outlet holes, PDMS channels were aligned to the electrode layer and brought into conformal contact. A 0.5% (w/w) Nafion™ solution diluted in 200 proof ethanol (Nafion™ 117 solution, Sigma-Aldrich, St. Louis, MO) was introduced into the microfluidic channel inlet using a micropipette. The device was placed under vacuum for 15 min to allow solvent evaporation, after which the PDMS channel was removed.

Glass channels were fabricated from 100 mm × 100 mm, 1.5-mm thick soda-lime glass/Cr mask blanks precoated with 5300-Å thick AZ1500 photoresist (Telic Co., Santa Clarita, CA). After laser writing (DWL 66+) and developing channel patterns (AZ® 400K developer, MicroChemicals GmbH), exposed Cr was etched using chrome etchant, and glass channels were isotropically etched to a depth of 100 µm using a solution of 49% (w/w) hydrofluoric acid (HF), 69% (w/w) nitric acid (HNO_3), and DI water in a volumetric ratio of 2:1:6. Residual photoresist and remaining Cr were removed by 10-min ozone plasma treatment (PE-50 Asher) and chrome etchant, respectively.

Electrode-array substrates and microfluidic channel superstrates were diced to final dimensions using a dicing saw (DAD 323, Disco Corporation, Tokyo, Japan). 1-mm diameter inlet and outlet holes were drilled into the channel layers using diamond-coated glass drill bits. After sonication in an acetone bath for 3 min and sequential rinsing with methanol, isopropanol, and DI water, residual moisture was removed from electrode and channel layers by drying under nitrogen flow and heating on a 120 °C hot plate for 15 min. Superstrates and substrates were bonded using a stamp-and-stick method with a UV-curable adhesive (NOA 61, Norland Products, East Windsor, NJ). Aligned and prebonded devices were cured for 45 min on a 60 °C hot plate and then held at room temperature for at least 72 h prior to use.

Assembled devices were mounted in a custom-designed microscopy-compatible 3D printed holder that offers individually addressable connections to each lead on the electrode layer via pogo-pins (825 spring-loaded pogo pin header strip, Mill-Maxx Mfg. Corp., Oyster Bay, NY) and press fit microfluidic inlet and outlet ports (NanoPort Kit for 1/16" OD tubing, IDEX Health and Science, Oak Harbor, WA) (Figure 1C(ii)).

2.2. Electrochemical Characterization of µ-BEC

2.2.1. Cyclic Voltammetry

The µ-BEC platform was electrochemically characterized using the ferricyanide/ferrocyanide redox couple ($[Fe(CN)_6]^{3-}/[Fe(CN)_6]^{4-}$). An aqueous solution of equimolar 1 mM potassium ferricyanide and potassium ferrocyanide in 1 M KCl, and a separate 1 M KCl solution for background current measurements were prepared. Both solutions were bubbled with a 50 kPa mixture of 80% N_2 and 20% CO_2 for 60 min to remove dissolved oxygen. Trapped air was eliminated from the microfluidic platform by introducing 1 mL of isopropyl alcohol at a flow rate of 10 µL/s using a syringe pump (Legato 110®, KD Scientific, Holliston, MA). 2.5 mL of 1 M KCl solution was flowed at 1 µL/s for background current measurement. Cyclic voltammograms were recorded under no-flow conditions using a multichannel potentiostat (PalmSens4 with MUX8-R2 Multiplexer, PalmSens, Houten, Netherlands) with the µ-BEC device mounted on the microscope stage inside a Faraday cage. Scan rates of 5, 10, 15, 20, and 25 mV/s were used, with three replicate measurements at each. Between

© 2026 by the author(s). Distributed under a Creative Commons CC BY license.

Preprints.org (www.preprints.org) | NOT PEER-REVIEWED | Posted: 13 April 2026 doi:10.20944/preprints202505.1879.v2

each measurement, 10 µL of fresh KCl solution was flowed at 1 µL/s. Following background measurements, 2.5 mL of 1 mM potassium ferricyanide/potassium ferrocyanide in 1 M KCl was introduced at a flow rate of 1 µL/min, and cyclic voltammetry was repeated under identical scan rate and loading conditions. To assess reproducibility, measurements were repeated on one electrode side across three separate µ-BEC devices.

Oxidation and reduction peaks were identified using MATLAB (MathWorks, Natick, MA), after subtraction of the average background current from the ferri/ferrocyanide voltammograms. Further data processing and statistical analysis were performed using Microsoft Excel (Microsoft Corporation, Redmond, WA) and MATLAB. Linear regression analysis was used to evaluate the dependence of peak current on the square root of the scan rate.

2.2.2. Differential Pulse Voltammetry

The concentration-dependent electrochemical response of the µ-BEC platform was evaluated using differential pulse voltammetry (DPV) measurements of the ferri/ferrocyanide redox couple across three wells of a single device. Equimolar aqueous solutions of potassium ferricyanide and potassium ferrocyanide in 1 M KCl were prepared at concentrations of 1, 10, 100, and 1000 µM. Solutions were bubbled with a 50 kPa mixture of 80% N_2 and 20% CO_2 for 60 min prior to use to remove dissolved oxygen.

Fluid delivery was managed using a pressure-based microfluidic control system comprising a pressure control unit (MFCS-EZ, Fluigent, Le Kremlin-Bicêtre, France), a flow sensor (Flow Unit, Fluigent), and an inline gas bubble trap (Elveflow, Paris, France). For each concentration, 2.5 mL of solution was introduced at a flow rate of 10 µL/s. Three replicate DPV scans were recorded per concentration per well, with 10 µL of fresh solution introduced at 1 µL/s between replicates. Concentrations were measured in ascending order, from lowest to highest. Before the complete set of ferri/ferrocyanide measurements at each concentration, 2.5 mL of 1 M KCl background solution was introduced at 10 µL/s and a fresh background voltammogram was recorded. The corresponding background subtraction was applied to all ferri/ferrocyanide voltammograms prior to analysis.

DPV scans were acquired using a multichannel potentiostat (PalmSens4, PalmSens). Anodic scans were recorded from +0.1 V to +0.5 V, and cathodic scans from +0.5 V to +0.1 V, each at a step potential of 10 mV/s with a pulse amplitude of 25 mV and a pulse duration of 0.3 s. All potentials are reported versus the on-chip Ag/AgCl/Nafion pseudoreference electrode.

Oxidation and reduction peak currents and potentials were identified using PS Trace Software (PalmSens). Concentration dependence of peak currents was evaluated by linear regression analysis in Microsoft Excel.

2.3. Culture and Characterization of the Model EEU Organism Rhodopseudomonas palustris TIE-1 inside the µ-BEC Platform

Isopropyl alcohol, ethyl alcohol, and basal freshwater medium were prepared in sterile glass serum bottles and purged with 50 kPa of 80% N_2 and 20% CO_2 for 30 min prior to use. A syringe pump (KD Scientific) was used to load one side of the µ-BEC platform with 1 mL of isopropyl alcohol at a flow rate of 10 µL/s to remove trapped gas bubbles, followed by 2.5 mL of ethyl alcohol for sterilization. The platform was left to sit with the ethyl alcohol solution for 30 min, after which it was flushed with 2.5 mL of purged freshwater medium at a flow rate of 10 µL/s.

Rhodopseudomonas palustris TIE-1 cells were cultured photoautotrophically in freshwater medium with 80% H_2 and 20% CO_2 in sealed 100 mL sterile glass serum bottles at 30 °C with illumination from a 60 W incandescent light bulb positioned ~25 cm above the bottles. Cultures were harvested when OD_{660} = 1.5, centrifuged at 5000 × g, washed three times with basal freshwater medium, and resuspended to final OD_{660} = 5.5. Prior to inoculation, the cell suspension was purged with 5 kPa of 80% N_2 and 20% CO_2 for 30 min.

Approximately 0.5 mL of concentrated TIE-1 culture was loaded into the µ-BEC platform inside an anaerobic chamber at a flow rate of 10 µL/min. The working electrodes were poised at +100 mV

© 2026 by the author(s). Distributed under a Creative Commons CC BY license.

Preprints.org (www.preprints.org) | NOT PEER-REVIEWED | Posted: 13 April 2026 doi:10.20944/preprints202505.1879.v2

vs. standard hydrogen electrode (SHE) for approximately 96 h under continuous illumination from a 60 W incandescent light bulb positioned ~25 cm above the platform to facilitate biofilm formation. After the incubation period, light-on/off chronoamperometry experiments were performed at 30-s intervals for a total of 300 s with three repeated measurements per electrochemical cell. After the initial light-on/off experiments, unattached and planktonic cells were removed by flushing the platform with 0.5 mL of freshwater medium (pre-purged with 5 kPa of 80% N_2 and 20% CO_2 for 30 min) at a flow rate of 10 µL/min inside the anaerobic chamber. Final light on/off chronoamperometry measurements were recorded as described previously. Chronoamperometry data were analyzed using MATLAB.

Brightfield transmitted light images of each µ-BEC unit were acquired using an inverted microscope (Axio Observer Z.1, Zeiss, Oberkochen, Germany) equipped with a 2.5× objective (EC Plan-NEOFLUAR 2.5×/0.085, WD = 8.8 mm, Zeiss) at multiple time points: before cell inoculation, after inoculation, after the 96-h incubation, and after planktonic cell removal.

3. Results and Discussion

3.1. Design and Fabrication of the µ-BEC Devices

Each µ-BEC device comprises a microfluidic channel layer and an electrode layer, both fabricated from glass to enable transmitted light optical imaging. Assembled devices contain eight individual three-electrode µ-BEC units arranged in a 2 × 4 layout (Figure 1A,C). A custom microscope-compatible metal-and-plastic holder provides individually addressable electrical connections to each electrode via spring-loaded pogo pins (Figure 1C(ii)).

µ-BEC units consist of three concentric electrodes patterned on the glass substrate (Figure 1A(i),(ii) and Figure 1C(i)): an indium tin oxide (ITO) working electrode (WE) for simultaneous electrochemical analysis and optical imaging, a gold counter electrode (CE), and a silver pseudoreference electrode (pRE). All electrodes incorporate Cr or Ti adhesion layers to promote film stability. The exposed surface areas of the WE, CE, and pRE are 1.96 mm^2, 5.93 mm^2, and 1.29 mm^2, respectively. These electrodes are enclosed within 4-mm diameter, 100-µm deep wells, isotropically etched into the microfluidic channel superstrate. To enable efficient flushing of non-adherent planktonic cells, each well is fluidically connected to its neighbors via 500-µm wide channels.

Electrode arrays were created using a lithography/metallization/lift-off approach adapted for microfabrication scalability and reproducibility. The two-step lift-off resist process improved edge definition and avoided incomplete lift-off (Chang and Kempisty 2003). The resultant undercut profile inhibited continuous sidewall coverage during material deposition, particularly for the sputtered films, and ensured clean removal of undesired material during lift-off. Here, overnight immersion in a remover solution without ultrasonication prevented redeposition of detached materials that can contaminate electrode surfaces and degrade system performance. While more time-intensive, this method also minimized particle residue and preserved electrode integrity. Finally, all electrodes were vacuum annealed at 320 °C to enhance adhesion, improve structural integrity, and reduce the risk of delamination (Lim et al. 2020).

The microfluidic wells and channels were created using wet-etching in fluorine-based chemistry. This inherently isotropic etching technique removed exposed glass equally in all directions, so the masking pattern accounted for feature expansion. In addition to hydrochloric acid, nitric acid was necessary to etch the lime (sodium oxide and calcium oxide) portion of the soda-lime glass. Sidewall roughness was controlled using the relative concentrations of the two acids, stirring pattern and frequency, as well as the quality of the masking layer (Iliescu et al. 2005; Iliescu et al. 2007). Rough sidewalls can contribute to observed gas bubble trapping and in future device iterations this can be mitigated by using lower etch rates or by switching to a pure silicon dioxide channel (Iliescu et al. 2005; Iliescu and Tay 2005; Iliescu et al. 2007).

Several considerations constrained how the two device layers were bonded. We avoided methods that might oxidize, thermally stress, or foul electrode surfaces. The system must withstand

© 2026 by the author(s). Distributed under a Creative Commons CC BY license.

Preprints.org (www.preprints.org) | NOT PEER-REVIEWED | Posted: 13 April 2026 doi:10.20944/preprints202505.1879.v2

long exposures to aqueous solutions and ethanol-based solutions for sterilization. Thus, plasma or high-temperature techniques were not considered. Laser-cut polymer-based adhesive layers were tested, but these failed under solvent treatment during sterilization or during aqueous exposure. Further, the laser-cut adhesives generated debris that fouled electrode surfaces when loaded with liquids. The stamp-and-stick method (Satyanarayana et al. 2005) allows for coating of the adhesive only over the non-etched area of the glass channels and relies on capillary forces for adhesion. SU-8 2005 photoresist was initially considered but the large contact area and poor wetting of the glass surface caused electrode fouling before the bonding surfaces were adequately covered. Thus, NOA 61 optical adhesive was selected for its superior affinity to glass.

To enhance the stability of the silver pseudoreference electrodes, the electrodes were chlorinated to form Ag/AgCl. Annealing conditions for improved adhesion (Lim et al. 2020) and wet chlorination (Kim et al. 2015) were adapted from reported methods for making thin-film Ag/AgCl electrodes to ensure selective modification. Selectivity for the pseudoreference electrodes was achieved by applying a protective photoresist layer over the CE and WE to prevent the modification of these surfaces. Following chlorination, the protective photoresist was removed by sequential acetone rinsing. The chlorination process is illustrated in Figure S1. Scanning electron microscopy (SEM) images document the expected morphological transitions to the pseudoreference electrodes before and after chlorination (Figure S3), confirming the transition of smooth Ag to granular AgCl structure consistent with previous reports (Kim et al. 2015; Lim et al. 2020).

To enhance the stability and longevity of the Ag/AgCl pseudoreference electrodes, a Nafion™ membrane was applied as a protective barrier. Nafion™ is a cation-exchange polymer that minimizes AgCl dissolution while preserving electrochemical functionality. Using polymeric coatings for thin-film pseudoreference electrodes for temporal stability and in-use protection has been established elsewhere (Shinwari et al. 2010). The stability of our pseudoreference electrodes was evaluated over a 120-h period, corresponding to the typical incubation and testing duration for EEU-capable bacteria previously reported in μ-BEC platforms (Gupta et al. 2021; Guzman et al. 2019). Long-term stability is considered essential for ensuring reliable electrochemical measurements and avoiding unwanted drift in electrode potentials. Here, pseudoreference electrode stability was assessed using open circuit potential (OCP) measurements conducted in freshwater media against standard Ag/AgCl/3 M KCl reference electrodes. Results are presented in Figure S4.

The pseudoreference electrodes exhibited an average potential drift of –0.30 mV/h, with a standard deviation of 0.06 mV/h, yielding a coefficient of variation (CV) of 20.7%. This drift exceeded the 0.09 mV/h reported in the reference study used for fabrication benchmarking (Lim et al. 2020), though the different testing media composition may have contributed to the observed discrepancy. Nonetheless, the measured drift fell within the midrange of values previously reported for similar electrodes (Shinwari et al. 2010). The electrodes began at an average potential of 167 mV (standard deviation: 4.54 mV, CV: 2.7%) and concluded at 131 mV (standard deviation: 8.82 mV, CV: 6.7%), corresponding to a net potential change of –36 mV over the 120-h testing period (standard deviation: 7.51 mV, CV: 21%). It is important to note that these measurements were performed relative to Ag/AgCl/3 M KCl reference electrodes, which themselves exhibit interelectrode variability of approximately ±20 mV and intrinsic potential drift in solution. Consequently, a portion of the observed potential change may reflect instability in the reference electrode rather than the pseudoreference electrodes under test.

Calibration of Ag/AgCl pseudoreference electrodes was performed to establish a consistent reference potential for interpreting electrochemical measurements. This step was necessary due to previously reported variability in the potential of microfabricated Ag/AgCl pseudoreference electrodes relative to commercial Ag/AgCl reference electrodes, with differences ranging from 0 to 270 mV (Shinwari et al. 2010). Calibration ensures that electrochemical data obtained from μ-BEC platforms can be referenced to standard electrochemical systems. Calibration results including representative cyclic voltammograms and comparative half-wave potentials are shown in Figure S5. Measurements were conducted sequentially in the same solution vessel using paired commercial and

© 2026 by the author(s). Distributed under a Creative Commons CC BY license.

Preprints.org (www.preprints.org) | NOT PEER-REVIEWED | Posted: 13 April 2026 doi:10.20944/preprints202505.1879.v2

pseudoreference electrodes. Commercial Ag/AgCl/3 M KCl reference electrodes exhibited an average half-wave potential of 214 ± 0.58 mV (CV: 0.27%), while microfabricated Ag/AgCl/Nafion™ pseudoreference electrodes displayed an average half-wave potential of 174 ± 5.5 mV (CV: 3.17%), corresponding to an average potential offset of –40 mV versus Ag/AgCl/3 M KCl. Although ideal calibration would involve in situ measurement using the ferri/ferrocyanide redox couple both before and after biotic experiments to account for potential drift, this approach was not feasible due to limitations in the current μ-BEC design. Because the ferri/ferrocyanide redox probe irreversibly modifies the working electrode surface and the probe is toxic to microbial cells, it cannot be used in live-cell experiments. While electrode fouling could be mitigated with use of a dedicated calibration electrode, addressing cytotoxicity requires the identification of a biocompatible redox standard. Despite these constraints, the low variability and drift observed in the pseudoreference electrode potentials suggest that the combined use of chemical chlorination and selective Nafion™ membrane protection yields consistent and durable reference electrodes for use in μ-BEC biological experiments.

3.2. Electrochemical Characterization of the μ-BEC Platform

3.2.1. Cyclic Voltammetry

The electrochemical behavior of the μ-BEC platform was first evaluated using the ferri/ferrocyanide redox couple as a well-established electrochemical probe to assess fundamental device performance. Figure 2 summarizes the electrochemical response of a representative well across multiple scan rates, with comparable behavior observed across all devices and wells tested (n = 3 devices x 4 wells). Cyclic voltammograms recorded at scan rates ranging from 5 to 25 mV/s exhibited well-defined anodic and cathodic peaks whose magnitudes increased systematically with increasing scan rate (Figure 2A). The preservation of peak shape and overall symmetry across scan rates indicates stable electrochemical behavior and consistent electrode performance within the microfluidic environment. Repeated scans at the same scan rate displayed overlapping peak shapes (Figure 2B).

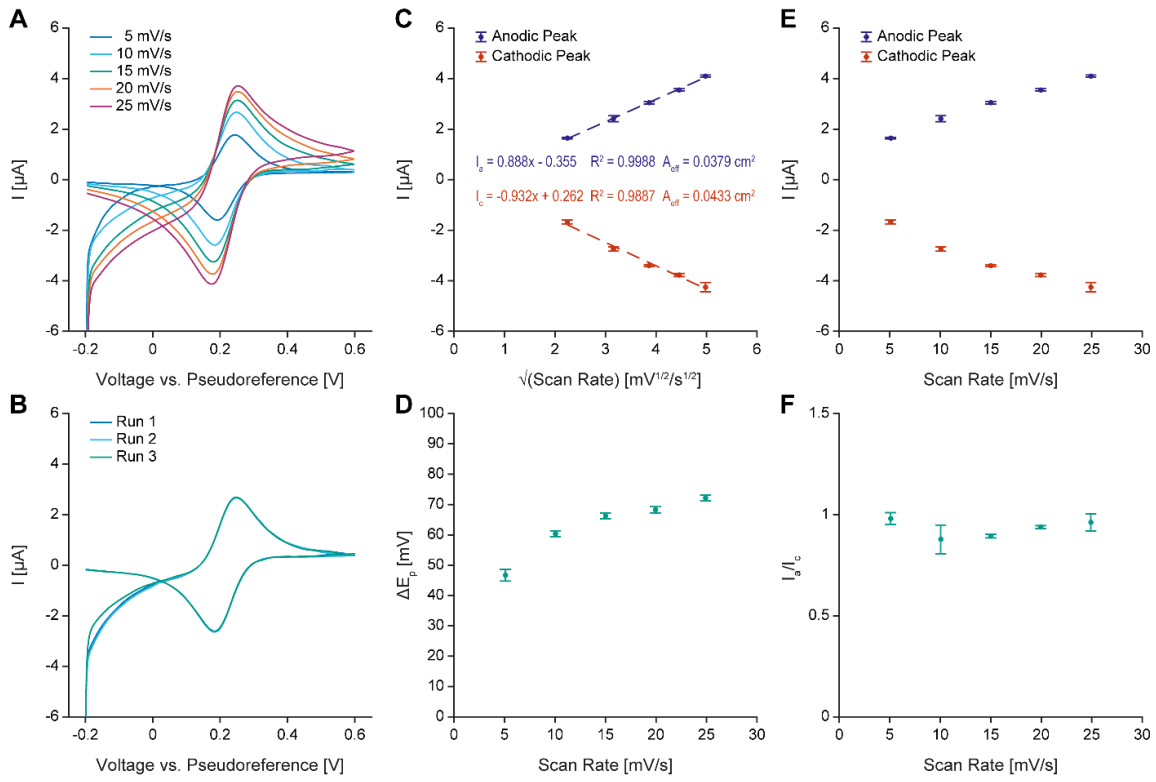

Figure 2. Electrochemical characterization of single μ-BEC well. (A) Representative cyclic voltammograms recorded at scan rates of 5, 10, 15, 20, and 25 mV s^{-1}. (B) Overlay of three consecutive cyclic voltammetry scans

© 2026 by the author(s). Distributed under a Creative Commons CC BY license.

Preprints.org (www.preprints.org) | NOT PEER-REVIEWED | Posted: 13 April 2026 doi:10.20944/preprints202505.1879.v2

at 10 mV/s (C) Anodic (I_{pa}) and cathodic (I_{pc}) peak currents plotted as a function of the square root of the scan rate, with mean ± SD shown across replicate scans and linear fits corresponding to the Randles–Ševčík relationship. Extracted effective electrochemical surface areas for anodic and cathodic processes are indicated. (D) Peak-to-peak separation (ΔE_p) as a function of scan rate, plotted as mean ± SD across replicate scans. (E) Anodic and cathodic peak currents plotted directly as a function of scan rate. (F) Ratio of anodic to cathodic peak currents as a function of scan rate, shown as mean ± SD.

Peak current analysis revealed a linear dependence of both anodic and cathodic peak currents on the square root of the scan rate (Figure 2C), consistent with diffusion-controlled mass transport as described by the Randles–Ševčík relationship. This behavior confirms that redox species transport within the μ-BEC device is governed by diffusion under the conditions tested and is not dominated by adsorption or surface-confined processes. Comparable linear trends were observed for both oxidation and reduction, supporting symmetric redox behavior at the electrode interface. Within individual devices, mean anodic effective areas ranged from 3.30 ± 0.14 mm² to 4.70 ± 0.31 mm² across the three devices, with well-to-well coefficients of variation between 4.2% and 8.1%. Mean cathodic effective areas ranged from 3.94 ± 0.12 mm² to 4.76 ± 0.20 mm², with well-to-well coefficients of variation between 1.6% and 4.1%. Across independently fabricated devices, anodic effective areas yielded a mean of 3.86 ± 0.74 mm² (CV: 19.1%) and cathodic areas a mean of 4.36 ± 0.41 mm² (CV: 9.4%). Notably, the extracted effective electrochemical surface areas exceeded the geometric working electrode area of 1.96 mm² by approximately twofold, which can be attributed to nanoscale roughness of the sputtered ITO thin films.

The separation between anodic and cathodic peak potentials (ΔE_p) increased with scan rate (Figure 2D), with values exceeding the theoretical limit for an ideal reversible one-electron system. However, the absence of abrupt changes and nonlinear dependence of current to scan rate (Figure 2E) suggest that kinetic limitations and ohmic losses remained stable across the examined range and that species adsorption at the working electrode surface did not dominate the electrochemical response. The ratio of anodic to cathodic peak currents remained close to one across all scan rates (Figure 2F), indicating balanced oxidation and reduction processes and minimal loss of electroactive species during cycling. Together, these results demonstrate predictable, diffusion-controlled electrochemical behavior with stable peak characteristics across scan rates.

To quantitatively assess well-to-well reproducibility within individual μ-BEC devices, anodic and cathodic peak currents, peak potentials, ΔE_p, and current ratios were compared across the four wells of each device. Figure 3 presents plots showing the mean ± SD values for a representative device at each scan rate, enabling direct visualization of inter-well variability within the device. Similar figures for the other independently fabricated devices tested for this study are presented in Figure S6 and Figure S7. Across all devices, anodic and cathodic peak potentials exhibited very low variability between wells. When averaged across scan rates, coefficients of variation for cathodic peak potential ranged from approximately 0.6% to 1.1%, while anodic peak potential coefficients of variation ranged from approximately 0.6% to 1.5% across the three devices. This low variability indicates a consistent electrochemical environment within each device and suggests stable reference electrode behavior. Peak currents exhibited higher variability across wells. When averaged across scan rates, coefficients of variation for cathodic peak current ranged from approximately 1.6% to 4.6%, while anodic peak current coefficients of variation ranged from approximately 4.6% to 8.4%. The observed variability in current magnitude was consistent with differences in effective electrochemical surface area between wells rather than differences in the underlying redox mechanism.

© 2026 by the author(s). Distributed under a Creative Commons CC BY license.

Preprints.org (www.preprints.org) | NOT PEER-REVIEWED | Posted: 13 April 2026 doi:10.20944/preprints202505.1879.v2

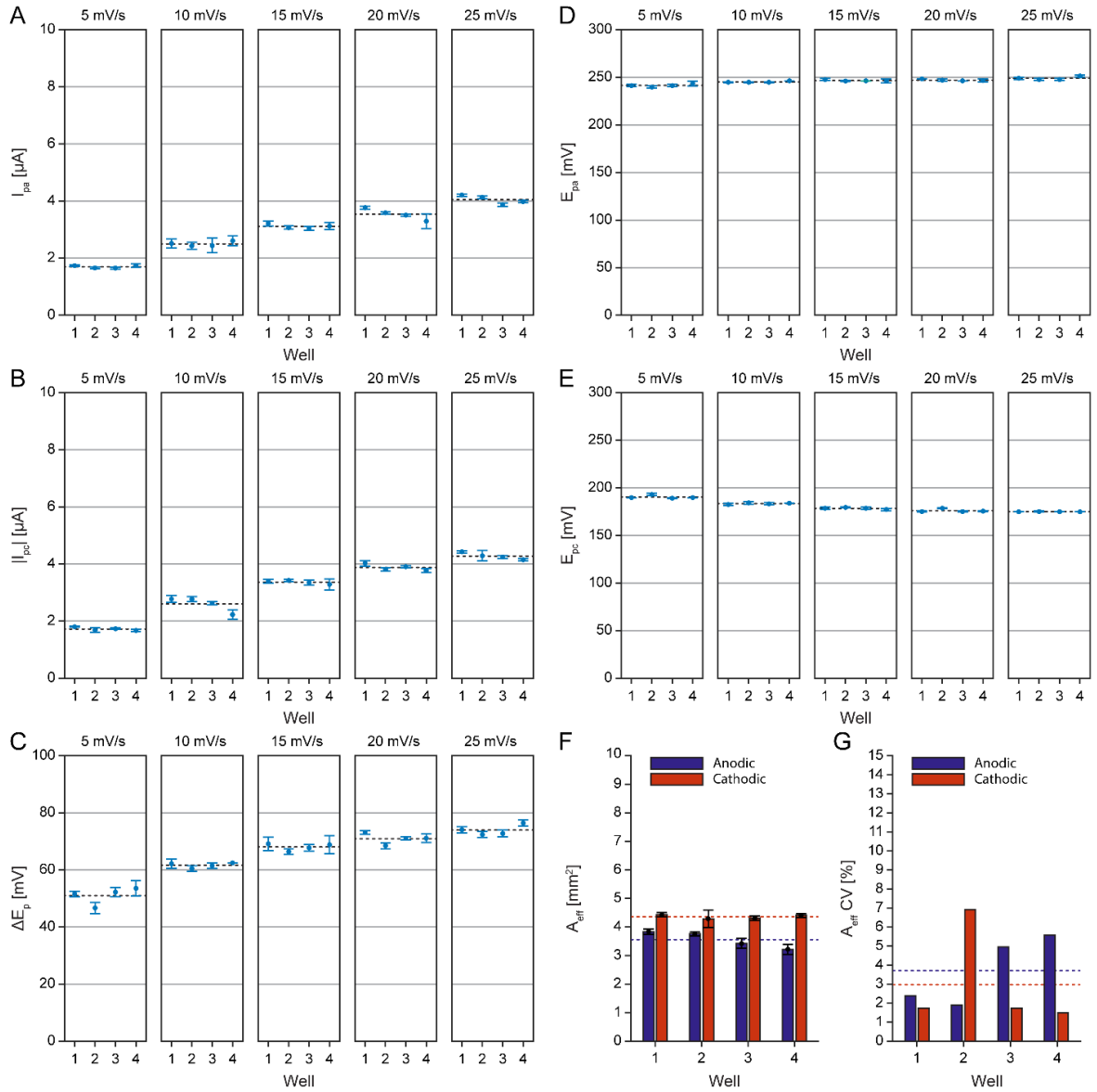

Figure 3. Well-to-well reproducibility of electrochemical metrics within a representative µ-BEC device. Scan-rate-dependent electrochemical parameters across the four wells of a representative device, with values shown as mean ± SD across 3 replicate scans for each well. (A) Anodic peak current (I_{pa}) and (B) absolute cathodic peak current ($|I_{pc}|$) as a function of well number for scan rates from 5 to 25 mV s^{-1}. (C) Peak-to-peak separation (ΔE_p) across wells at each scan rate. (D) Anodic peak potential (E_{pa}) and (E) cathodic peak potential (E_{pc}) across wells. (F) Effective surface area extracted from Randles–Ševčík analysis for anodic and cathodic processes, shown as mean ± SD across scan rates for each well. (G) Coefficients of variation (CV) for anodic and cathodic effective surface area, summarizing well-to-well variability within the device.

Device-to-device reproducibility was evaluated by comparing peak currents and peak potentials across three independently fabricated µ-BEC devices. Figure 4 summarizes anodic and cathodic peak potentials, peak currents, and effective electrochemical surface areas and their coefficients of variation, with values averaged across all wells within each device. Peak potentials were highly consistent across devices, with coefficients of variation of approximately 1.8% for anodic peaks and 1.6% for cathodic peaks when averaged across scan rates. This low inter-device variability highlights robust reference electrode performance and reliable potential control across independently fabricated devices. In contrast, greater variability was observed in peak currents across devices. Coefficients of variation for anodic and cathodic peak currents were approximately 9.5% and 13.5%, respectively, reflecting device-to-device differences in absolute current magnitude. Transient obstruction of electrode surfaces by gas bubbles within the microfluidic environment may have reduced the

© 2026 by the author(s). Distributed under a Creative Commons CC BY license.

Preprints.org (www.preprints.org) | NOT PEER-REVIEWED | Posted: 13 April 2026 doi:10.20944/preprints202505.1879.v2

electrochemically active area in some devices, contributing to current variability without substantially affecting peak potential.

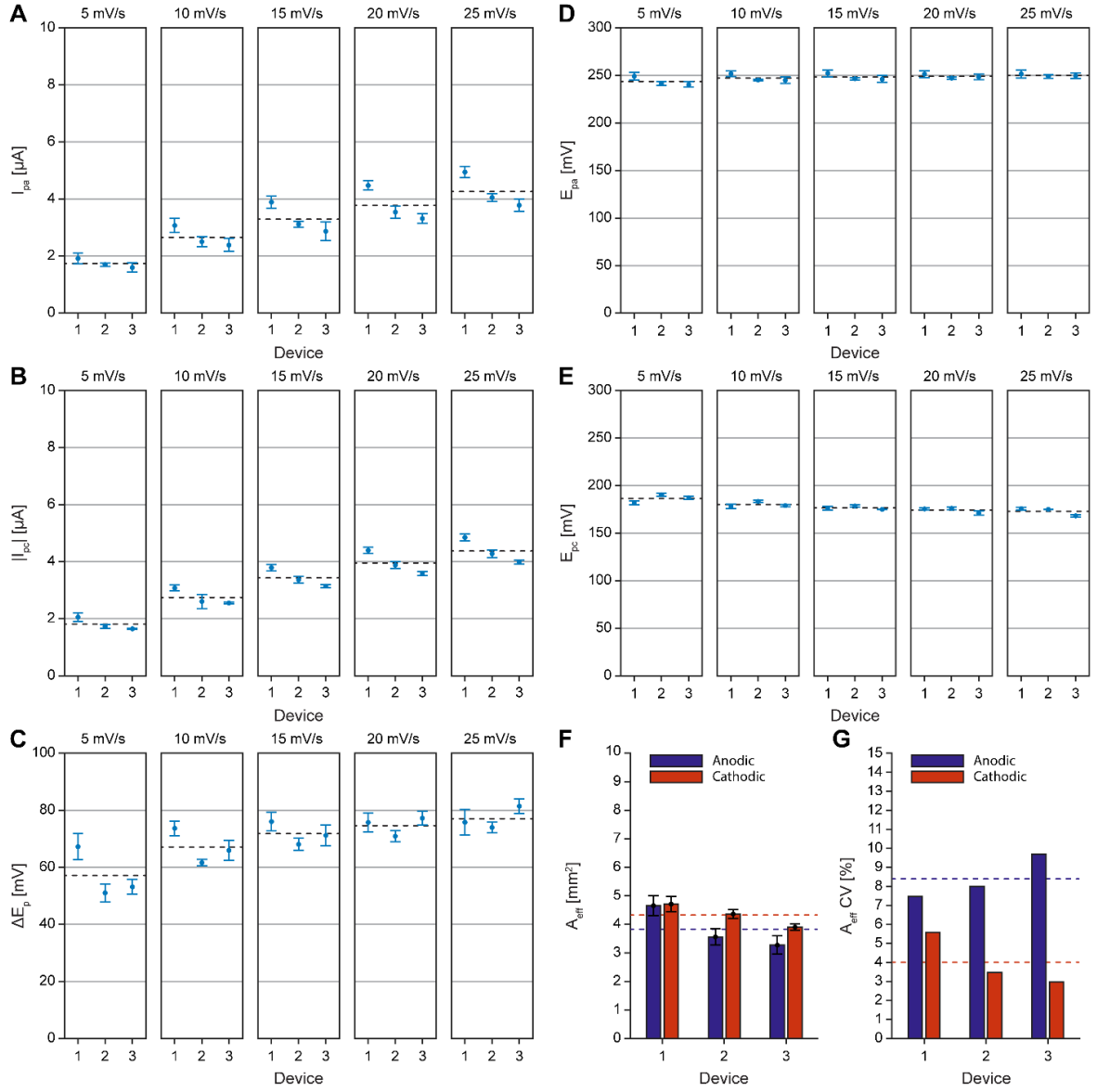

Figure 4. Device-to-device reproducibility of electrochemical performance across independently fabricated µ-BEC devices. Scan-rate-dependent electrochemical parameters across three independently fabricated µ-BEC devices, with values shown as mean ± SD averaged across all wells within each device. (A) Anodic peak current (I_{pa}) and (B) absolute cathodic peak current ($|I_{pc}|$) plotted as a function of device number for scan rates from 5 to 25 mV s^{-1}. (C) Peak-to-peak separation (ΔE_p) across devices at each scan rate. (D) Anodic peak potential (E_{pa}) and (E) cathodic peak potential (E_{pc}) across devices. (F) Effective surface area extracted from Randles–Ševčík analysis for anodic and cathodic processes, shown as mean ± SD across scan rates for each device. (G) Coefficients of variation (CV) for anodic and cathodic effective surface area, summarizing device-to-device variability.

Overall, the µ-BEC platform exhibits well-defined and reproducible electrochemical behavior both across the wells within a device and between independently fabricated devices. The low variability in peak potentials underscores stable reference electrode operation and consistent potential control, while the larger variability in peak currents is attributable primarily to differences in electrochemically active surface area. Together, these results establish a robust and reproducible electrochemical baseline for the µ-BEC platform, providing a solid foundation for subsequent studies of spatial uniformity, device-to-device reproducibility, and sensing performance in more complex experimental environments.

© 2026 by the author(s). Distributed under a Creative Commons CC BY license.

Preprints.org (www.preprints.org) | NOT PEER-REVIEWED | Posted: 13 April 2026 doi:10.20944/preprints202505.1879.v2

3.2.2. Differential Pulse Voltammetry

Differential pulse voltammetry (DPV) was used to evaluate the concentration-dependent electrochemical response of the μ-BEC platform using the ferri/ferrocyanide redox couple. Figure 5 presents representative DPV responses over a concentration range from 1 μM to 1 mM, including anodic and cathodic scans. Well-defined anodic and cathodic peaks were observed, with peak current magnitudes increasing with increasing concentration (Figure 5A,B). The observed shift in both anodic and cathodic peak potentials toward more negative values with increasing concentration can be attributed to a concentration-dependent shift in the formal potential of the ferri/ferrocyanide redox couple. Additionally, the use of pseudoreference electrodes may contribute to the observed potential shift, as the potential of thin-film electrodes is sensitive to the ionic composition of the surrounding solution, unlike conventional reference electrodes with a fixed internal electrolyte.

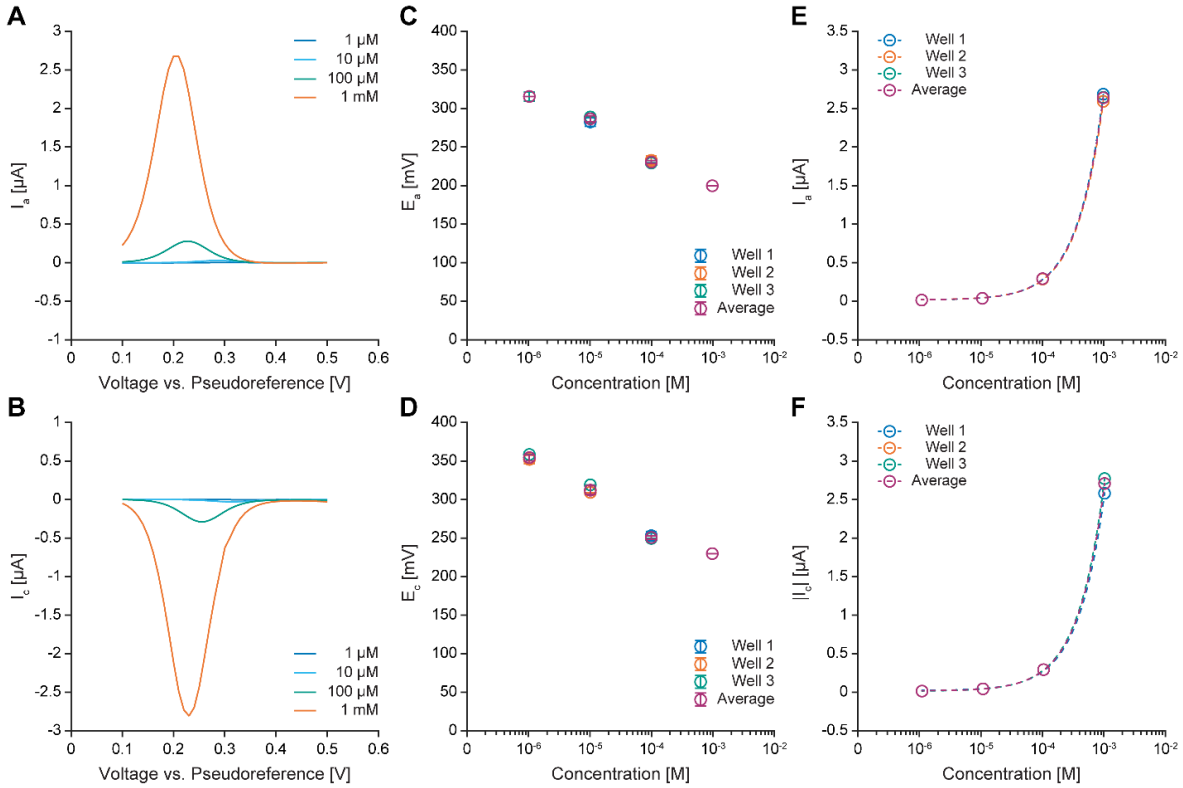

Figure 5. Differential pulse voltammetry (DPV) characterization of concentration-dependent electrochemical response in the μ-BEC platform. Representative DPV current–potential traces acquired at concentrations of 1, 10, 100, and 1000 μM are shown for the anodic (A) and cathodic (B) scans. (C) Anodic peak potential (E_{pa}) and (D) cathodic peak potential (E_{pc}) plotted as a function of concentration, with values shown as mean ± SD across replicate measurements for each cell and the overall mean across cells. (E) Anodic peak current (I_{pa}) and (F) absolute cathodic peak current ($|I_{pc}|$) plotted as a function of concentration on logarithmic axes, with mean values shown for each cell and linear regression fits overlaid.

The concentration dependence of peak potentials is summarized in Figure 5C,D. Anodic peak potentials shifted from a mean of 0.317 V at 1 μM to 0.200 V at 1 mM, while cathodic peak potentials shifted from 0.356 V to 0.230 V over the same concentration range. Peak currents plotted as a function of concentration (Figure 5E,F) show a linear increase for both anodic and cathodic processes across all tested cells. Anodic peak currents increased from a mean of 2.69 ± 0.09 nA at 1 μM to 2.65 ± 0.05 μA at 1 mM, and cathodic peak currents increased in magnitude from 2.76 ± 0.11 nA to 2.72 ± 0.10 μA over the same range. While the limited number of concentration points prevents the determination of analytical sensitivity or detection limits, these results demonstrate that the μ-BEC platform supports reproducible, concentration-dependent DPV sensing under abiotic conditions.

© 2026 by the author(s). Distributed under a Creative Commons CC BY license.

Preprints.org (www.preprints.org) | NOT PEER-REVIEWED | Posted: 13 April 2026 doi:10.20944/preprints202505.1879.v2

3.3. Characterization of the Model EEU Organism Rhodopseudomonas palustris TIE-1 inside the μ-BEC Platform

To demonstrate the compatibility of the μ-BEC platform with biological EEU measurements, *Rhodopseudomonas palustris* TIE-1 was used as a model phototrophic EEU organism (Guzman et al. 2019). Figure 6 presents a representative light-on/off chronoamperometric response from a single μ-BEC well, comparing measurements acquired in the presence and absence of planktonic cells, along with corresponding brightfield microscopy images collected at different experimental stages and average current uptake values. Consistent with earlier work, illuminated conditions showed increased cathodic current uptake compared with dark intervals. Removal of planktonic cells by controlled microfluidic flushing resulted in a reduction of the light-induced current response, which indicates light-dependent extracellular electron uptake. The reduction in current raises the possibility that planktonic cells contribute meaningfully to the measured electron uptake. Confirming this interpretation requires further studies with appropriate controls, particularly to account for potential partial disruption of surface-attached biofilms by shear forces during microfluidic flushing, which could independently account for the observed current reduction.

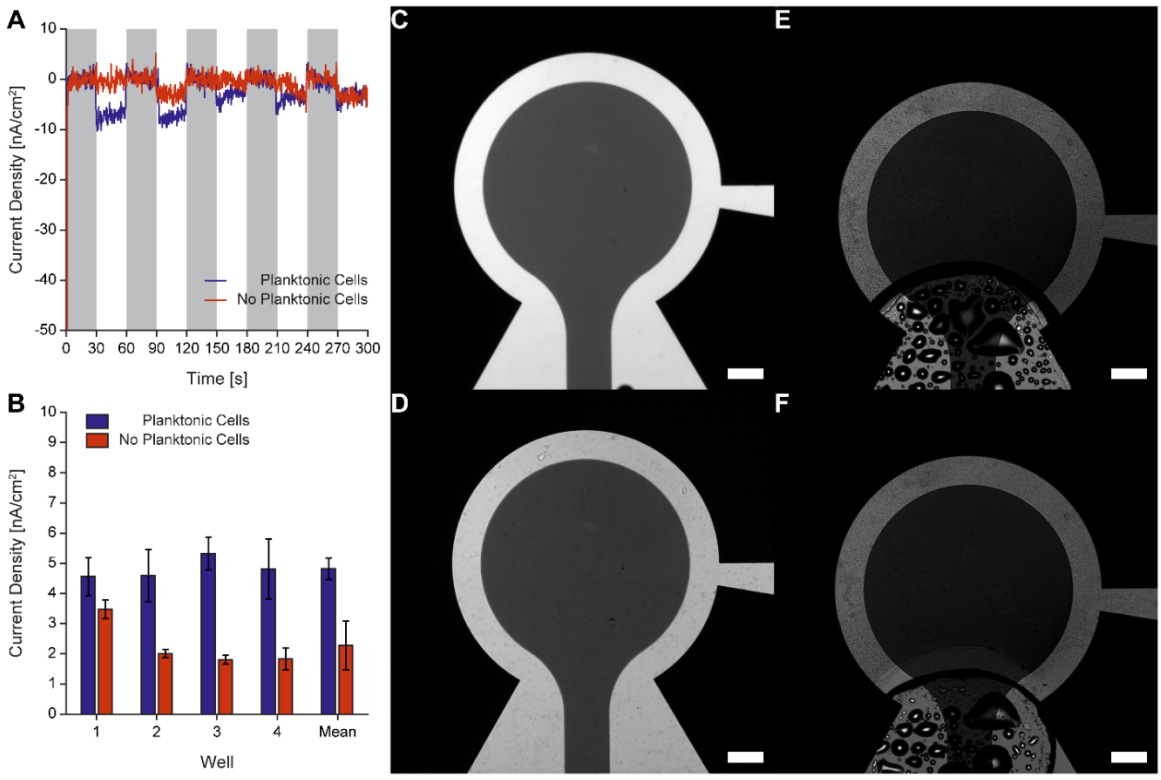

Figure 6. TIE-1 behavior in the μ-BEC platform. (A) Representative normalized light on/off chronoamperometric current density traces. Shaded regions indicate light-off periods. (B) Mean current density uptake quantified across individual wells, shown as mean ± SD for conditions with and without planktonic cells, demonstrating a reduced electrochemical response in the absence of planktonic cells. (C–F) Brightfield images of a representative μ-BEC well different stages of the experiment: (C) prior to inoculation, (D) immediately after inoculation, (E) after incubation, and (F) after removal of planktonic cells. Scale bar: 250 μm.

Quantification of the mean current uptake across wells revealed variability in absolute current magnitude, attributed in part to gas bubble formation and persistence within the microfluidic chambers during inoculation and early operation. Brightfield microscopy (Figure 6C-F) showed routine gas bubble formation within wells and over the working electrode surfaces, likely obstructing the electrode areas and creating growth heterogeneity by modulating the degree of microbial attachment on the working electrode surface. The measured current densities displayed in Figure 6B were approximately an order of magnitude lower than those previously reported for TIE-1 in related

© 2026 by the author(s). Distributed under a Creative Commons CC BY license.

Preprints.org (www.preprints.org) | NOT PEER-REVIEWED | Posted: 13 April 2026 doi:10.20944/preprints202505.1879.v2

platforms from our group (Guzman et al. 2019). This difference may partly reflect the reduced well volume of the μ-BEC (~1.26 μL) compared to previously used devices (~4.79 μL), a ~3.8-fold difference. The smaller solution volume available per unit electrode area in the μ-BEC may restrict nutrient availability and carbon dioxide diffusion to the biofilm, potentially suppressing overall EEU activity.

Despite the observed variability in absolute current magnitude across wells, the qualitative electrochemical response remained consistent, with light-dependent current uptake observed both before and after removal of planktonic cells. The microscopy images corroborate the electrochemical measurements, capturing the progression from a clean electrode surface before cell loading to the retention of surface-attached cell films after planktonic cell removal. Together, these results demonstrate that the μ-BEC platform supports light-dependent microbial electron uptake measurements, while identifying gas bubble formation and removal as important engineering considerations for future platform optimization.

4. Conclusion

The reported work presents a scalable, glass-based microfluidic bioelectrochemical cell platform designed to support reproducible, multiplexed electrochemical measurements in microscale environments. While existing microfluidic bioelectrochemical platforms, including PDMS, polymer, and paper or textile-based devices, have proven valuable for rapid prototyping, low-cost, and proof-of-concept demonstrations, they present inherent limitations in long-term chemical stability, optical transparency, and fabrication reproducibility that can constrain their broader deployment. The μ-BEC addresses these limitations by building entirely on glass using standard photolithographic, wet-etch, and thin-film deposition processes compatible with wafer-scale batch fabrication, enabling consistent production of multiple devices per wafer with defined electrode geometries, stable reference electrodes, and integrated microfluidic control within a single monolithic platform. The use of industry-compatible processes, including lift-off metallization, wet isotropic glass etching, and UV-adhesive bonding, provides a clear pathway toward higher-density array configurations and broader deployment beyond the individual research laboratory.

Through systematic electrochemical characterization using the ferri/ferrocyanide redox couple, the platform exhibited predictable, diffusion-controlled behavior that was highly reproducible across wells and independently fabricated devices. Coefficients of variation for anodic and cathodic peak potentials ranged from approximately 0.6 to 1.5% across wells within a device and 1.6 to 1.8% across independently fabricated devices, confirming stable reference electrode performance and consistent potential control. The larger variability observed in peak currents with coefficients of variation ranging from 1.6 to 8.4% between wells within a device and 9.5 to 13.5% between independently fabricated devices is consistent with expected differences in effective electrode area arising from microfabrication tolerances and the presence of obstructing gas bubbles, rather than from instability in the underlying electrochemistry. The ability of the μ-BEC platform to support concentration-dependent electrochemical sensing was validated using differential pulse voltammetry, where anodic and cathodic peak currents exhibited linear dependence on ferri/ferrocyanide concentration across a three-order-of-magnitude range from 1 μM to 1 mM. While detailed sensitivity and detection limit analyses were beyond the scope of this study, these results demonstrate the platform's suitability for DPV-based sensing applications.

To validate biotic compatibility, the μ-BEC platform successfully detected light-dependent EEU in the phototrophic bacterium *Rhodopseudomonas palustris* TIE-1 under chronoamperometric conditions, consistent with prior reports for this organism. Variability in absolute current magnitude across wells, attributable to gas bubble formation within the microfluidic chambers, highlights an important engineering challenge for future platform optimization rather than a limitation of the underlying electrochemical functionality.

Together, these results establish the μ-BEC as a robust, reproducible, and manufacturable microscale electrochemical platform that enables parallelized measurements and supports multiple

© 2026 by the author(s). Distributed under a Creative Commons CC BY license.

Preprints.org (www.preprints.org) | NOT PEER-REVIEWED | Posted: 13 April 2026 doi:10.20944/preprints202505.1879.v2

electrochemical techniques multiplexed with optical imaging. Additionally, the use of wafer-scale fabrication processes provides a strong foundation for future scale-up and deployment in high-throughput investigations of microbial electrochemical behavior.

Supplementary Materials: The following supporting information can be downloaded at the website of this paper posted on Preprints.org.

Acknowledgments: This work was supported by the following grants to J.M.M.: DEPSCoR grant FA9550-21-1-0211 and National Institutes of Health R01GM141344. Additional support from grants to A.B.: The David and Lucile Packard Foundation Fellowship (201563111), the U.S. Department of Energy (grant number DESC0014613), and the U.S. Department of Defense, Army Research Office (grant number W911NF-18-1-0037), Gordon and Betty Moore Foundation, National Science Foundation (grant numbers 2021822, 2124088, 2117198, and 2300081), the U.S. Department of Energy by Lawrence Livermore National Laboratory under Contract DEAC5207NA27344 (LLNL-JRNL-812309). A.B. was also funded by a Collaboration Initiation Grant, an Office of the Vice Chancellor of Research Grant, an International Center for Energy, Environment, and Sustainability Grant and a SPEED grant from Washington University in St. Louis. This work was also supported by the National Science Foundation under NSF-CAREER 1846005 and National Institutes of Health 1R35GM158225-01 to J.A.V.B.

Author Contributions: A.S.: Conceptualization, Data curation, Formal analysis, Investigation, Methodology, Validation, Writing – original draft, Writing – review & editing. K.R.: Conceptualization, Methodology, Validation, Writing – review & editing. T.R.: Investigation (cell culture), Validation, Writing – review & editing. J.A.V.B.: Funding acquisition, Project administration, Supervision, Validation, Writing – review & editing. A.B.: Conceptualization, Funding acquisition, Project administration, Supervision, Validation, Writing – review & editing. J.M.M.: Conceptualization, Funding acquisition, Project administration, Supervision, Validation, Writing – review & editing.

Data Availability: The data supporting the findings of this study are available from the corresponding authors upon reasonable request.

Conflicts of Interest: The authors declare no conflicts of interest.

References

Amirdehi, M.A., Gong, L., Khodaparastasgarabad, N., Sonawane, J.M., Logan, B.E., Greener, J., 2022. Hydrodynamic interventions and measurement protocols to quantify and mitigate power overshoot in microbial fuel cells using microfluidics. Electrochimica Acta 405, 139771.

Battat, S., Weitz, D.A., Whitesides, G.M., 2022. An outlook on microfluidics: the promise and the challenge. Lab on a Chip 22(3), 530-536.

Chang, S.-C., Kempisty, J.M., 2003. Lift-off Methods for MEMS Devices. MRS Online Proceedings Library 729(1), 23.

Cho, H.-M., Ha, H., Ahn, Y., 2022. Co-laminar Microfluidic Microbial Fuel Cell Integrated with Electrophoretically Deposited Carbon Nanotube Flow-Over Electrode. ACS Sustainable Chemistry & Engineering 10(5), 1839-1846.

Cologgi Dena, L., Speers Allison, M., Bullard Blair, A., Kelly Shelly, D., Reguera, G., 2014. Enhanced Uranium Immobilization and Reduction by Geobacter sulfurreducens Biofilms. Applied and Environmental Microbiology 80(21), 6638-6646.

Conners, E.M., Rengasamy, K., Bose, A., 2022. Electroactive biofilms: how microbial electron transfer enables bioelectrochemical applications. Journal of Industrial Microbiology and Biotechnology 49(4), kuac012.

Franks, A.E., Nevin, K.P., 2010. Microbial Fuel Cells, A Current Review. Energies, pp. 899-919.

Gong, L., Khodaparastasgarabad, N., Hall, D.M., Greener, J., 2022. A new angle to control concentration profiles at electroactive biofilm interfaces: Investigating a microfluidic perpendicular flow approach. Electrochimica Acta 431, 141071.

© 2026 by the author(s). Distributed under a Creative Commons CC BY license.

Preprints.org (www.preprints.org) | NOT PEER-REVIEWED | Posted: 13 April 2026 doi:10.20944/preprints202505.1879.v2

Gupta, D., Guzman, M.S., Rengasamy, K., Stoica, A., Singh, R., Ranaivoarisoa, T.O., Davenport, E.J., Bai, W., McGinley, B., Meacham, J.M., Bose, A., 2021. Photoferrotrophy and phototrophic extracellular electron uptake is common in the marine anoxygenic phototroph Rhodovulum sulfidophilum. The ISME Journal 15(11), 3384-3398.

Guzman, M.S., Rengasamy, K., Binkley, M.M., Jones, C., Ranaivoarisoa, T.O., Singh, R., Fike, D.A., Meacham, J.M., Bose, A., 2019. Phototrophic extracellular electron uptake is linked to carbon dioxide fixation in the bacterium Rhodopseudomonas palustris. Nature Communications 10(1), 1355.

Iliescu, C., Jing, J., Tay, F.E.H., Miao, J., Sun, T., 2005. Characterization of masking layers for deep wet etching of glass in an improved HF/HCl solution. Surface and Coatings Technology 198(1), 314-318.

Iliescu, C., Tay, F.E., 2005. Wet etching of glass. CAS 2005 Proceedings. 2005 International Semiconductor Conference, 2005., pp. 35-44. IEEE.

Iliescu, C., Tay, F.E.H., Miao, J., 2007. Strategies in deep wet etching of Pyrex glass. Sensors and Actuators A: Physical 133(2), 395-400.

Karthikeyan, R., Singh, R., Bose, A., 2019. Microbial electron uptake in microbial electrosynthesis: a mini-review. Journal of Industrial Microbiology and Biotechnology 46(9-10), 1419-1426.

Khodaparastasgarabad, N., Couture, M., Greener, J., 2024. A microfluidic study of acetate conversion kinetics in a microbial electrolysis cell: The role of age, concentration and flow on biofilm permeability. Sensors and Actuators B: Chemical 412, 135779.

Kim, J., Kong, H.G., Ahn, Y., 2024. Textile-Based Membraneless Microfluidic Double-Inlet Hybrid Microbial–Enzymatic Biofuel Cell. ACS Applied Materials & Interfaces 16(33), 43661-43669.

Kim, T.Y., Hong, S.A., Yang, S., 2015. A Solid-State Thin-Film Ag/AgCl Reference Electrode Coated with Graphene Oxide and Its Use in a pH Sensor. Sensors 15(3), 6469-6482.

Kwon, Y., Hong, D., Ahn, Y., 2024. Monolayer textile-based co-laminar flow biocompatible enzymatic biofuel cell. Energy Conversion and Management 301, 118042.

Lee, C.H., Ha, H., Ahn, Y., Liu, H., 2023. Performance of single-layer paper-based co-laminar flow microbial fuel cells. Journal of Power Sources 580, 233456.

Lim, H.-R., Hillman, N., Kwon, Y.-T., Kim, Y.-S., Choa, Y.-H., Yeo, W.-H., 2020. Ultrathin, long-term stable, solid-state reference electrode enabled by enhanced interfacial adhesion and conformal coating of AgCl. Sensors and Actuators B: Chemical 309, 127761.

Lovley, D.R., 2006. Bug juice: harvesting electricity with microorganisms. Nature Reviews Microbiology 4(7), 497-508.

Lovley, D.R., Holmes, D.E., 2022. Electromicrobiology: the ecophysiology of phylogenetically diverse electroactive microorganisms. Nature Reviews Microbiology 20(1), 5-19.

Lovley, D.R., Nevin, K.P., 2013. Electrobiocommodities: powering microbial production of fuels and commodity chemicals from carbon dioxide with electricity. Current Opinion in Biotechnology 24(3), 385-390.

Lovley, D.R., Phillips, E.J.P., Gorby, Y.A., Landa, E.R., 1991. Microbial reduction of uranium. Nature 350(6317), 413-416.

Lovley, D.R., Stolz, J.F., Nord, G.L., Phillips, E.J.P., 1987. Anaerobic production of magnetite by a dissimilatory iron-reducing microorganism. Nature 330(6145), 252-254.

Nevin Kelly, P., Woodard Trevor, L., Franks Ashley, E., Summers Zarath, M., Lovley Derek, R., 2010. Microbial Electrosynthesis: Feeding Microbes Electricity To Convert Carbon Dioxide and Water to Multicarbon Extracellular Organic Compounds. mBio 1(2), 10.1128/mbio.00103-00110.

Park, N.H., Kim, J., Ahn, Y., 2023. Fabric-based self-pumping, single-stream microfluidic fuel cell. Electrochimica Acta 446, 142106.

Parkhey, P., Sahu, R., 2021. Microfluidic microbial fuel cells: Recent advancements and future prospects. International Journal of Hydrogen Energy 46(4), 3105-3123.

Pinck, S., Ostormujof, L.M., Teychené, S., Erable, B.A.-O., Microfluidic Microbial Bioelectrochemical Systems: An Integrated Investigation Platform for a More Fundamental Understanding of Electroactive Bacterial Biofilms. LID - 10.3390/microorganisms8111841 [doi] LID - 1841(2076-2607 (Print)).

© 2026 by the author(s). Distributed under a Creative Commons CC BY license.

Preprints.org (www.preprints.org) | NOT PEER-REVIEWED | Posted: 13 April 2026 doi:10.20944/preprints202505.1879.v2

Ranaivoarisoa, T.O., Singh, R., Rengasamy, K., Guzman, M.S., Bose, A., 2019. Towards sustainable bioplastic production using the photoautotrophic bacterium Rhodopseudomonas palustris TIE-1. Journal of Industrial Microbiology and Biotechnology 46(9-10), 1401-1417.

Sackmann, E.K., Fulton, A.L., Beebe, D.J., 2014. The present and future role of microfluidics in biomedical research. Nature 507(7491), 181-189.

Satyanarayana, S., Karnik, R.N., Majumdar, A., 2005. Stamp-and-stick room-temperature bonding technique for microdevices. Journal of Microelectromechanical Systems 14(2), 392-399.

Shi, L., Dong, H., Reguera, G., Beyenal, H., Lu, A., Liu, J., Yu, H.-Q., Fredrickson, J.K., 2016. Extracellular electron transfer mechanisms between microorganisms and minerals. Nature Reviews Microbiology 14(10), 651-662.

Shinwari, M.W., Zhitomirsky, D., Deen, I.A., Selvaganapathy, P.R., Deen, M.J., Landheer, D., 2010. Microfabricated reference electrodes and their biosensing applications. Sensors (Basel) 10(3), 1679-1715.

Tahernia, M., Mohammadifar, M., Gao, Y., Panmanee, W., Hassett, D.J., Choi, S., 2020a. A 96-well high-throughput, rapid-screening platform of extracellular electron transfer in microbial fuel cells. Biosensors and Bioelectronics 162, 112259.

Tahernia, M., Mohammadifar, M., Hassett, D.J., Choi, S., 2019. A fully disposable 64-well papertronic sensing array for screening electroactive microorganisms. Nano Energy 65, 104026.

Tahernia, M., Mohammadifar, M., Hassett, D.J., Choi, S., 2020b. A portable papertronic sensing system for rapid, high-throughput, and visual screening of bacterial electrogenicity. Biosensors and Bioelectronics 165, 112348.

Yang, Y., Ye, D., Li, J., Zhu, X., Liao, Q., Zhang, B., 2016. Microfluidic microbial fuel cells: from membrane to membrane free. Journal of Power Sources 324, 113-125.

Zarabadi, M.P., Paquet-Mercier, F., Charette, S.J., Greener, J., 2017. Hydrodynamic Effects on Biofilms at the Biointerface Using a Microfluidic Electrochemical Cell: Case Study of Pseudomonas sp. Langmuir 33(8), 2041-2049.

Disclaimer/Publisher's Note: The statements, opinions and data contained in all publications are solely those of the individual author(s) and contributor(s) and not of MDPI and/or the editor(s). MDPI and/or the editor(s) disclaim responsibility for any injury to people or property resulting from any ideas, methods, instructions or products referred to in the content.

© 2026 by the author(s). Distributed under a Creative Commons CC BY license.